Predictive simulation of concurrent debris flows: How slope failure locations affect predicted damage

AUTHOR(S):

Yamanoi, Kazuki; Oishi, Satoru; Kawaike, Kenji; Nakagawa, Hajime

ORIGINAL ARTICLE

Predictive simulation of concurrent debris flows: How slope failure locations affect predicted damage

Kazuki Yamanoi[1,2] 🔘 | **Satoru Oishi[2]** | **Kenji Kawaike[1]** | **Hajime Nakagawa[1]**

[1]Disaster Prevention Research Institute, Kyoto University, Kyoto, Japan

[2]RIKEN Center for Computational Science, Kobe, Hyogo, Japan

Correspondence
Kazuki Yamanoi, Disaster Prevention Research Institute, Kyoto University, Shimomisu-higashinokuchi, Yoko-oji, Fushimi-ku, Kyoto, Kyoto 6128235, Japan.
Email: yamanoi.kazuki.6s@kyoto-u.ac.jp

Funding information
FOCUS Establishing Supercomputing Center of Excellence; Japan Society for the Promotion of Science, Grant/Award Number: 19K15105

Abstract

Predictive simulation of concurrent debris flows using only pre-disaster information has been difficult, partly because of problems faced in predicting debris-flow initiation locations (i.e., slope failure). However, because catchment topography has convergent characteristics with all channels in it joining each other as they flow downstream, damage to downstream areas could be predicted using relatively inaccurate initiation points. Based on this hypothesis, this study uses debris-flow initiation points generated randomly with statistical slope failure prediction and performs a many-case simulation across numerous initiation points to quantify the effect of slope-failure locations in terms of deviations in the predicted water level and topographic change. This paper presents the results of 2D simulations based on a conventional debris-flow model that was run on a supercomputer to realise simulations of many cases. The obtained relative standard deviation was found to decrease as the debris flow and sediment-laden flood approached the downstream area, indicating that the predictability of the inundation and topographic change can be decided from the terrain characteristics.

KEYWORDS
debris flow, flash flood, sediment, uncertainty analysis

1 | INTRODUCTION

Debris flow is a primary hazard to human life (Hungr et al., 2014). When significant rainfall events affect a watershed topography, multiple debris flows occur concurrently within a single catchment. Additionally, debris flows and sediment-laden floods transported downstream with increasing discharge can significantly influence lowland areas. Numerical simulations are useful for reproducing such debris flows, assessing their risk, and designing countermeasures against them (Hungr & McDougall, 2009; Naef et al., 2006; O'Brien et al., 1993; Salvatici et al., 2017). In such simulations, post-disaster information, especially the location of debris-flow initiation, is crucial. However, locations of debris-flow initiation are unknown before the event, making predictive pre-disaster simulations difficult. Therefore, although such predictive simulations are essential to quantify the flood risk under debris flows and sediment-laden floods, especially in a high-risk catchment, assumptions are required to treat debris-flow initiation.

1.1 | Treatment of debris-flow initiation in existing simulations

From a physical viewpoint, three types of debris-flow initiation have been considered: (1) fluidization of a shallow

A Self-archived copy in
Kyoto University Research Information Repository
https://repository.kulib.kyoto-u.ac.jp

京都大学

KYOTO UNIVERSITY

2 of 18

WILEY—CIWEM
Chartered Institution of
Water and Environmental
Management

Journal of
Flood Risk Management

KURENAI 紅
Kyoto University Research Information Repository

YAMANOI ET AL.

landslide, (2) collapse of a natural dam comprising land-slide mass, and (3) erosion of river bed material by over-land flow (Takahashi, 2007). As debris-flow initiation includes many unknowns resulting from a lack of in situ observations, multiple assumptions are made in simulations. The first approach is to assume hydrograph and sediment concentration values at the inlet of the target domain (Bao et al., 2019; Chen et al., 2017; Frank et al., 2015; Gao et al., 2016; Han et al., 2018; Nakatani et al., 2016; Rickenmann et al., 2006). The inlet point is usually set as the debris-flow initiation point or the location where the debris flow is sufficiently developed. The simulation can then be simplified even if all elementary processes (e.g., rainfall infiltration, landslides, and debris-flow development) are neglected. However, hydrograph setting basically requires empirical variables or information that can only be obtained after an event, such as the total debris-flow volume (Rickenmann, 1999), and is difficult when considering multiple sources.

The second approach involves connecting a rainfall-infiltration-runoff simulation to a surface erosion model (Melo et al., 2018; van Asch et al., 2014). Although it precisely treats debris-flow initiation type (3), it requires multiple parameters related to water transportation (e.g., coefficient of saturated/unsaturated permeability), underground structures, and soil strength (e.g., cohesion coefficient, internal friction angle). These widely distributed physical underground parameters generally cannot be uniquely determined at the watershed scale, and no well-established remote observation techniques are available for obtaining them. Thus, this method is unsuitable for predictive simulations.

The third approach is to set the free-flowing landslide mass at the slope failure location (Revellino et al., 2004; Rodríguez-Morata et al., 2019; Schraml et al., 2015). Although it can treat only the initiation type (1), it requires fewer parameters than the second approach. For a debris flow that develops by eroding the slope surface material, initial landslide volume has a limited effect on debris-flow discharge (Hussin et al., 2012). Then, the distance between the slope failure and damaged area will be sufficiently large; therefore, accurate simulations should be possible using this methodology, if sufficient slope failure location data are available.

Separately, many studies have aimed to obtain the landslide susceptibility for landslide prediction. Approaches for generating landslide susceptibility maps include geomorphological mapping, analysis of landslide inventories, heuristic or index-based approaches, process-based (physically based) methods, and statistically based modelling (Reichenbach et al., 2018). Of these, physically and statistically based modelling are preferred for quantitative evaluation (Reichenbach et al., 2018). Physically based models afford advantages in terms of physical

validity; among them, the infinite slope stability model is a simplified, widely used approach (An et al., 2016; Raia et al., 2014). Although obtaining reliable results requires accurately modelling complicated, heterogeneous underground structures through field observation or parameter fitting using landslide records, it is not always necessary to use difficult-to-obtain physical parameters in statistically based approaches. Provided that reliable landslide records are used to obtain the statistical relationships, no abnormal results should be produced. If we can combine the simulation of debris-flow initiated from landslide mass with statistical landslide prediction, predictive debris-flow simulation with the identification of the susceptible area might become possible.

1.2 | Study area and target event

A typical case involving multiple concurrent debris flows and sediment-laden flood occurred on Northern Kyushu Island, Japan, in July 2017. Heavy rains induced multiple landslides, producing debris flows in the Akatani river catchment, Asakura city, Fukouoka prefecture, Japan (Figure 1). Subsequently, massive amounts of sediment covered a residential area located at the bottom of the valley. Sediment was also transported several kilometers downstream and deposited to a ~150-m width through a 10-m-width channel. The sediment-laden flood damaged both channel sides and areas far from the main channels. The disaster killed 33 people and damaged 1046 buildings throughout Asakura city (Fukuoka Prefecture, 2018). Notably, this event produced sediment from multiple landslides and associated debris flows, which strongly affected the inundation processes. Large topographic changes around channels caused by the flood produced severe damage (see Figure 2). Figure 3(a) shows the inundation area and slope failure traces, and (b) shows a hazard map (Fukuoka Prefecture, n.d.; Chikugo River Office, n.d.) published before the disaster event that included the inundation, slope failure, and debris-flow areas. Inundation and slope failure/debris-flow areas in this map were predicted separately, nothing is predicted in the intermediate region. However, heavy inundation occurred in the region because of the deposition of sediment transported from slope failures and associated debris flows.

According to the disaster report (Kyoto University, 2018), the slope failure depth was ~1–3 m. The boundary of the shallow landslides and debris flow is not clear; thus, this value seems to express both the landslide depth and erosion depth of the debris flow around the source. According to radar observations, the maximum total rainfall exceeded 700 mm, and the area in which total rainfall exceeded 650 mm is roughly spatially comparable with the area of
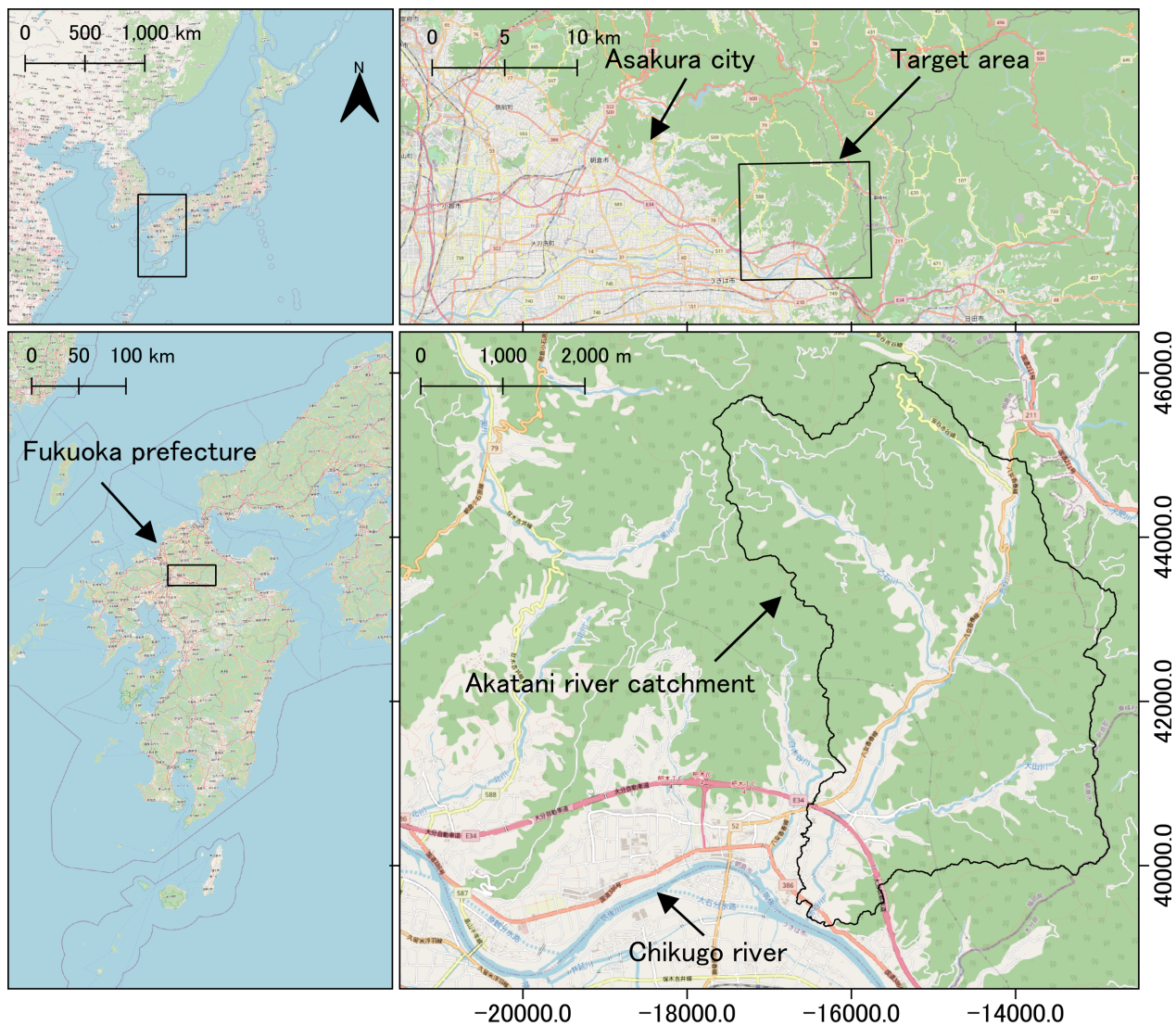
FIGURE 1 Geographical location of the target domain located in Asakura city, Fukuoka prefecture, Japan (OpenStreetMap Contributors, 2020)

concentrated shallow landslides (Kyoto University, 2018). Danjo et al. (2018) spatially analysed the relationship between the slope failure source and topographic characteristics and reported that the source areas of surface landslides are more likely to have occurred in ridge-like terrain than in valley-like terrain.

Overall, the following phenomena can be assumed. First, multiple landslides occurred in a short duration (i.e., order of several hours). Each slope failure mass was transformed into a debris flow and developed by eroding sediments on the slope surface. Therefore, almost all sediment along the channels eroded completely. Consequently, surface material erosion, and not initial landslide mass volume, mainly accounted for the sediment volume transported by debris flow. Compared to the initial volume, the slope failure location should greatly influence the total volume because the amount of erodible sediment changes depending on how upstream/

downstream debris flow initiates. However, in events with multiple debris flows, the effect of location can be reduced as downstream flows converge. That is, the watershed topography has a convergent characteristic; tributaries aggregate as they flow downwards; thus, debris flows of similar scales can result even if the initiation points (i.e., landslide location) change within a catchment. Therefore, the required accuracy of the initiation points for debris-flow simulation is also an important factor.

1.3 | Objective

The first study objective is to achieve a predictive simulation of the 2017 event using pre-disaster information. We assume that only the disaster scale (i.e., how large the disaster event will be, or how densely the debris flow

京都大学
KYOTO UNIVERSITY
4 of 18

A Self-archived copy in
Kyoto University Research Information Repository
https://repository.kulib.kyoto-u.ac.jp

KURENAI 紅
京都大学学術情報リポジトリ
Kyoto University Research Information Repository

YAMANOI ET AL.

WILEY—CIWEM Chartered Institution of Water and Environmental Management | Journal of Flood Risk Management

FIGURE 2 Damage in downstream area of Akatani river catchment (extracted from video captured by Geospatial Information Authority of Japan, 2017). The location of this picture is indicated by the red arrow in Figure 3(a)

initiate) in the target region is known, and the debris-flow source location in the target region and area affected by the debris flow and associated sediment-laden flood are unknown. We statistically estimate the debris-flow initiation location and simulate the transportation and inundation of debris flow and sediment-laden flood from this point. Notably, this is not a complete prediction because it excludes the estimation of the disaster scale. However, this can be predicted by a statistical approach using past disaster records, observational precipitation data, and so forth. Therefore, complete predictions could become possible by integrating this approach herein.

The second objective is to quantify the effect of the slope failure (i.e., debris-flow initiation points) location on the predicted inundation area of debris flow and sediment-laden flood. Thus, different slope failure patterns generated by the same statistical model are summarised and used as inputs for simulation. This study discusses the required accuracy in terms of debris-flow initiation location.

2 | SIMULATION METHODOLOGY

A supercomputer is used to simulate multiple simultaneous debris flows. Code availability and ease of editing were important factors in this regard; although several simulation software is already available, we developed a new simulation code. In general, debris-flow simulations can be

classified into Eulerian method employing shallow-water equations (SWE) (e.g., RAMMS; Christen et al., 2010; Hussin et al., 2012), FLO-2D (D'Agostino & Tecca, 2006; O'Brien et al., 1993; O'Brien & Julien, 1985), and D-Claw (George & Iverson, 2014; Iverson & George, 2014)) and Lagrangian methods, such as smoothed particle hydrodynamics (e.g., DAN3D; Hungr & McDougall, 2009). The Eulerian method has an advantage in applicability for parallel computing. From a physical viewpoint, RAMMS employs the Voellmy relationship, FLO2D employs the Bingham fluid model, and D-Claw employs a quasi-two-phase granular-fluid model. In Japan, a dilatant fluid model, which assumes stony-type debris flows (Takahashi, 2007), is usually applied for the simulation of debris flow. Takahashi (2007) expanded his model to simulate not only debris flows but also the state of immature debris and water flow including bed load transport. The target event of the current study included heavy inundation in downstream areas, which has a relatively lower density as compared to the upstream debris flow; therefore, we employed the expanded model by Takahashi (2007).

2.1 | Governing equations

To treat a debris flow, we selected a two-dimensional simulation model based on the widely used dilatant fluid model developed by Takahashi (2007) (Nakatani et al., 2016; Wu et al., 2013). The governing equation is
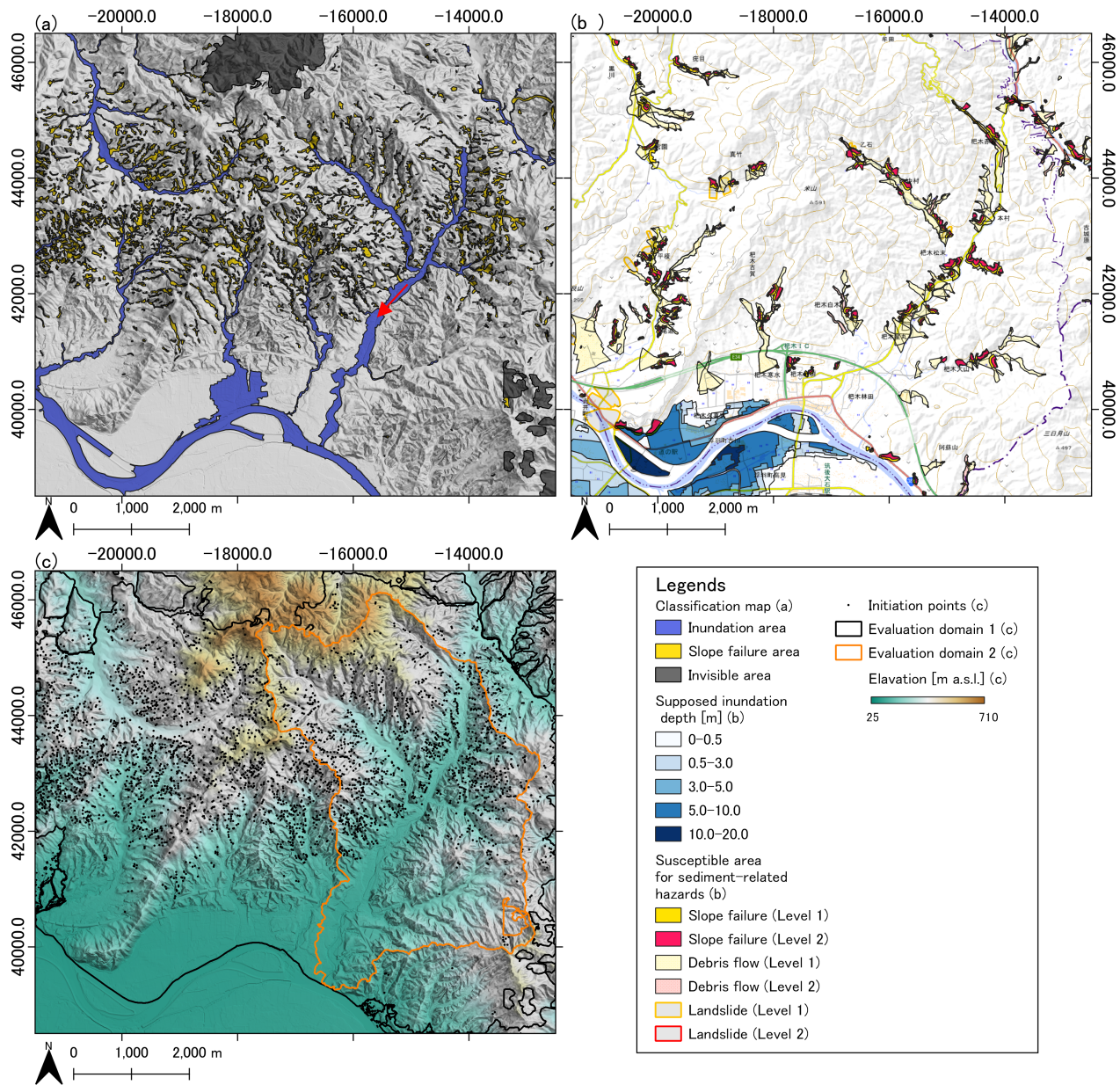
京都大学
KYOTO UNIVERSITY
YAMANOI ET AL.

CIWEM Chartered Institution of Water and Environmental Management | Journal of Flood Risk Management —WILEY

京都大学学術情報リポジトリ
KURENAI 紅
Kyoto University Research Information Repository
5 of 18

FIGURE 3 (a) Classification map of affected area produced by the 2017 Northern Kyushu Heavy Rainfall Disaster (Geospatial Information Authority of Japan, 2017). Red arrow indicates the location shown in Figure 2. (b) Supposed inundation area and affected area of sediment-related hazards in hazard map (Fukuoka Prefecture, n.d.; Chikugo River Office, n.d.). (c) 5-m-resolution elevations (Geospatial Information Authority of Japan, n.d.) and debris-flow initiation points ($n = 3721$) in target area for input into reproductive simulation. Domain for the quantitative evaluation in Section 3 is also shown here. Coordinate system on (a–c) follows Japan Plane Rectangular CS II (EPSG:2444)

$$\frac{\partial \boldsymbol{U}}{\partial t} + \frac{\partial \boldsymbol{E}}{\partial x} + \frac{\partial \boldsymbol{F}}{\partial y} = \boldsymbol{S}, \tag{1}$$

where U is the conservative variable vector; E and F are the flux vectors in the x- and y-directions, respectively; and S is the source vector. This equation is an integrated form of SWE and sediment transport equation, comprising the volumetric conservation law of fluids (debris flow), momentum equations for x- and y-directions,

volumetric conservation law of sediment concentration in fluid, and land-surface material conservation law.

The vectors are defined as

$$\mathbf{U} = \begin{pmatrix} h \\ uh \\ vh \\ Ch \\ z_b \end{pmatrix}, \mathbf{E} = \begin{pmatrix} uh \\ u^2h + \frac{1}{2}gh^2 \\ uvh \\ Cuh \\ 0 \end{pmatrix}, \mathbf{F} = \begin{pmatrix} vh \\ uvh \\ v^2h + \frac{1}{2}gh^2 \\ Cvh \\ 0 \end{pmatrix},$$

京都大学
KYOTO UNIVERSITY
6 of 18
WILEY—CIWEM Chartered Institution of Water and Environmental Management
Journal of Flood Risk Management

京都大学学術情報リポジトリ
KURENAI 紅
Kyoto University Research Information Repository
YAMANOI ET AL.

$$\mathbf{S} = \begin{pmatrix} i \\ gh(S_{0x} - S_{fx}) + \dfrac{\partial}{\partial x}\left\{\epsilon\dfrac{\partial(uh)}{\partial x}\right\} + \dfrac{\partial}{\partial y}\left\{\epsilon\dfrac{\partial(uh)}{\partial y}\right\} \\ gh(S_{0y} - S_{fy}) + \dfrac{\partial}{\partial x}\left\{\epsilon\dfrac{\partial(vh)}{\partial x}\right\} + \dfrac{\partial}{\partial y}\left\{\epsilon\dfrac{\partial(vh)}{\partial y}\right\} \\ iC_* \\ -i, \end{pmatrix}, \quad (2)$$

where h is the depth of water or water-sediment mixture (m); u and v are the depth-averaged velocities (m/s) in the x- and y-directions, respectively; C is the sediment concentration in the fluid (−); z_b is the land-surface elevation (m); g is the acceleration due to gravity (m/s^2); i is the erosion speed (m/s) calculated using Equation (5); C_* is the sediment concentration (−) in the soil at the ground surface. The topographical gradients in the x- and y-directions are, respectively, calculated as $S_{0x} = \partial z_b / \partial x$ and $S_{0y} = \partial z_b / \partial y$. ϵ is the eddy momentum diffusivity (m^2/s) and is calculated as

$$\epsilon = \frac{1}{6}\kappa u_* h, \quad (3)$$

where κ is von Karmans' constant (−); u_* is the frictional velocity (m/s); S_{fx} and S_{fy} are frictional gradients between the fluid and bed surface in the x- and y-directions (−), respectively. To consider both debris flow and sediment-laden flooding, the three-phase (stony debris, hyperconcentrated, and water flow) model proposed by Takahashi and Nakagawa (1991) is used:

$$S_{fx} = \begin{cases} \dfrac{u\sqrt{u^2+v^2}d^2}{8gh^3\left\{C+(1-C)\frac{\rho}{\sigma}\right\}\left\{\left(\frac{C_*^{1/3}}{C}\right)-1\right\}}, & C \geq 0.4C_* \\ \dfrac{u\sqrt{u^2+v^2}d^2}{0.49gh^3}, & 0.01 \leq C < 0.4C_* \\ \dfrac{n_m^2 u\sqrt{u^2+v^2}}{h^{4/3}}, & C < 0.01 \end{cases},$$

$$S_{fy} = \begin{cases} \dfrac{v\sqrt{u^2+v^2}d^2}{8gh^3\left\{C+(1-C)\frac{\rho}{\sigma}\right\}\left\{\left(\frac{C_*^{1/3}}{C}\right)-1\right\}}, & C \geq 0.4C_* \\ \dfrac{v\sqrt{u^2+v^2}d^2}{0.49gh^3}, & 0.01 \leq C < 0.4C_* \\ \dfrac{n_m^2 u\sqrt{u^2+v^2}}{h^{4/3}}, & C < 0.01 \end{cases}$$

$$(4)$$

where d is the representative sediment diameter (m) and n_m is Manning's roughness coefficient (m$^{-1/3}$s). The three phases are treated separately by comparing the sediment densities in fluid C and river bed C_*. The erosion/

deposition velocity in the vertical direction i is calculated as

$$i = \begin{cases} \delta_e \dfrac{C_\infty - C}{C_* - C_\infty}\dfrac{h\sqrt{u^2+v^2}}{d}, & C_\infty \geq C \\ \delta_d \dfrac{C_\infty - C}{C_*}\sqrt{u^2+v^2}, & C_\infty < C \end{cases} \quad (5)$$

where δ_e and δ_d are the empirically defined coefficients for erosion and deposition (−), respectively, that provide the time required for transition to the equilibrium condition (i.e., $C = C_\infty$) (Takahashi, 2007). ρ and σ are the specific weights of water and sediment, respectively. Positively valued i expresses the erosion speed (m^2/s), where C_∞ is the equilibrium sediment concentration (−) obtained by

$$C_\infty = \begin{cases} 0.9C_*, & \tan\theta_w \geq \tan\phi \\ \dfrac{\rho\tan\theta_w}{(\sigma-\rho)(\tan\phi-\tan\theta_w)}, & \tan\phi > \tan\theta_w \geq 0.138 \\ 6.7\left\{\dfrac{\rho\tan\theta_w}{(\sigma-\rho)(\tan\phi-\tan\theta_w)}\right\}^2, & 0.138 > \tan\theta_w \geq 0.03 \\ \dfrac{\rho(1+5\tan\theta_w)}{\rho-\sigma}\left(1-\alpha_c^2\dfrac{\tau_{*c}}{\tau_*}\right)\left(1-\alpha_c\sqrt{\dfrac{\tau_{*c}}{\tau_*}}\right), & \tan\theta_w \leq 0.03 \wedge \tau_* > \tau_{*c} \\ 0, & \tan\theta_w \leq 0.03 \wedge \tau_* \leq \tau_{*c} \end{cases}$$

$$(6)$$

where θ_w is the water surface gradient (−). In this study, we used the gradient in the downstream direction. ϕ is the internal friction angle (−); τ_{*c} is the critical non-dimensional tractive force (−) calculated as

$$\tau_{*c} = 0.04 \times 10^{1.72\tan\theta_w}, \quad (7)$$

where τ_* is the nondimensional tractive force calculated as

$$\tau_* = \frac{\rho}{\sigma-\rho}\frac{h\tan\theta_w}{d}, \quad (8)$$

where α_c is calculated as

$$\alpha_c^2 = \frac{2\left(0.425 - \frac{\sigma\tan\theta_w}{\sigma-\rho}\right)}{1 - \frac{\sigma\tan\theta_w}{\sigma-\rho}} \quad (9)$$

2.1.1 | Numerical modelling

To prevent numerical instability at the boundary of supercritical and subcritical flows, the MacCormack scheme with artificial viscosity (Hinokidani, 1998a) is used to implement the discretisation equations. Calculations are performed in two steps: prediction and

京都大学
KYOTO UNIVERSITY
YAMANOI ET AL.

A Self-archived copy in
Kyoto University Research Information Repository
https://repository.kulib.kyoto-u.ac.jp

CIWEM Chartered Institution of Journal of
Water and Environmental Flood Risk Management—WILEY
Management

京都大学学術情報リポジトリ
KURENAI 紅
Kyoto University Research Information Repository
7 of 18

correction. If backward and forward differences are used for the predictor and collector steps, respectively, the MacCormack scheme can be expressed as follows:

Predictor:

$$\overline{U}_{i,j} = U_{i,j}^n - \frac{\Delta t}{\Delta x}\left\{\left(E_{i,j}^n - E_{i-1,j}^n\right) - \left(Q_{xi,j}^n - Q_{xi-1,j}^n\right)\right\} - \frac{\Delta t}{\Delta y}\left\{\left(F_{i,j}^n - E_{i,j-1}^n\right) - \left(Q_{yi,j}^n - Q_{yi,j-1}^n\right)\right\} + \Delta t S_{i,j}^n.$$

(10)

Corrector:

$$U_{i,j}^{n+1} = \frac{1}{2}\left(U_{i,j}^n + \overline{U}_{i,j}\right) - \frac{\Delta t}{2\Delta x}\left\{\left(\overline{E}_{i+1,j} - \overline{E}_{i,j}\right) + \left(\overline{Q}_{xi+1,j} - \overline{Q}_{xi,j}\right)\right\} - \frac{\Delta t}{2\Delta y}\left\{\left(\overline{F}_{i,j+1} - \overline{F}_{i,j}\right) + \left(\overline{Q}_{yi,j+1} - \overline{Q}_{yi,j}\right)\right\} + \frac{1}{2}\Delta\overline{S}_{i,j},$$

(11)

where

$$Q_{xi,j} = \frac{u_* h}{\Delta x}K_v\left(U_{i+1,j}^n - 2U_{i,j}^n + U_{i-1,j}^n\right),$$
$$Q_{yi,j} = \frac{u_* h}{\Delta y}K_v\left(U_{i,j+1}^n - 2U_{i,j}^n + U_{i,j-1}^n\right)$$

(12)

where K_v is the coefficient vector for artificial viscosity; $K_v = [2.5, 2.5, 2.5, 1, 1]$ was used in this study (Hinokidani, 1998b).

As the initial condition, a debris-flow mass consisting of water and sediment was set at four nearest grid cells (i.e., 10 m × 10 m) corresponding to the debris-flow initiation points. The mass has depth h and concentration C, and does not have momentum (i.e., $u = v = 0$). First, the initial vectors $\boldsymbol{U}^{n0}$, $\boldsymbol{E}^{n0}$, $\boldsymbol{F}^{n0}$ in timestep $n = n_0$ are set using Equation (2). Further, $\boldsymbol{S}$ and $\boldsymbol{Q}$ are calculated using the components of $\boldsymbol{U}$ (i.e., u, v, h, C, and z_b) using Equations (3)–(9) and (12). Next, in the predictor step, vector $\overline{\boldsymbol{U}}$ is calculated by Equation (10). $\overline{\boldsymbol{U}}$ is calculated by substituting it into $\boldsymbol{U}$ in Equation (2), and $\overline{\boldsymbol{E}}$, $\overline{\boldsymbol{F}}$, $\overline{\boldsymbol{S}}$, and $\overline{\boldsymbol{Q}}$ are calculated using $\overline{\boldsymbol{U}}$ and its components similar to the previous step. In the corrector step, vectors $\boldsymbol{U}^{n0+1}$ are obtained using Equation (10) and the above vectors. Then, time t (s) is incremented by Δt. Debris flow transportation and erosion/deposition is calculated in such time steps.

2.1.2 | Code parallelisation

A Fortran numerical simulation code was used for performing the above calculations. As applying this programme

at a watershed scale could incur high computational costs, we parallelised the code to enable the use of high-performance computing techniques (supercomputing).

Hence, we introduced thread-parallelisation to the programme using OpenMP, a technique for parallelising programme loops. This enabled the parallelisation of most loops without causing dependency problems. To execute the programme on supercomputers comprising multiple nodes, we implemented message passing interface (MPI) parallelisation, in which a target area is decomposed into multiple areas overlapping two arrays of numerical grids. In this study, the target area is separated into 288 square areas of 100 × 100 computing cells (i.e., 500 × 500 m); we then added overlapping cells along the boundary of the decomposed area. Each area is allocated to corresponding nodes, and the simulation is executed independently on each node. Using MPI, the variables on overlapping grids were synced just after the predictor and collector steps to retain collective variables on the boundary area. Through this hybrid parallelisation process, a one-case simulation of a rectangular domain of 8 km × 9 km could successfully be conducted on 2304 CPU cores (288 nodes, eight cores per node) in less than 2000 s; for the full study, a 60-case parallel simulation was conducted using 138,240 cores (17,280 nodes, eight cores per node). This simulation was performed on the K computer at the RIKEN Center for Computational Science, Kobe, Japan.

3 | REPRODUCTIVE SIMULATION

3.1 | Calculation condition

To validate the proposed simulation scheme, we applied it to an actual disaster that occurred on Northern Kyushu Island, Japan, in 2017. The target region was an area spanning 9 and 8 km in the east–west and north–south directions, respectively, around the Akatani river catchment area. The simulation is conducted in a 5 m-resolution spatial discretization; thus, number of grid cells was 2,880,000. While a 10-m resolution DEM was fully available in the target domain, a 5-m resolution DEM was partially available in the residential area. Therefore, we upscaled the 10-m-resolution DEM by bicubic interpolation to complement the 5-m DEM. We also converted the polygonal debris-flow traces provide by Geospatial Information Authority of Japan (2017) into a point dataset of debris-flow initiation as follows. We defined the debris-flow initiation point in each debris flow trace as the highest point. As most debris-flow traces joined each other, we assumed that the highest-elevation cells were the high points within a specific diameter for the debris-flow trace. Figure 3(c) shows the resulting

8 of 18 | WILEY—CIWEM Chartered Institution of Water and Environmental Management Journal of Flood Risk Management

A Self-archived copy in
Kyoto University Research Information Repository
https://repository.kulib.kyoto-u.ac.jp

KURENAI 紅
Kyoto University Research Information Repository

YAMANOI ET AL.

debris-flow initiation points ($n = 3721$) and elevation data for the simulation. For other parameters, pure water and general sediment condition ($\rho = 1.0, C_* = 0.6, \sigma = 2.65, \phi = 35°$) were used. The target area has a wide grain size distribution of 0.04–100.00 mm (Kyoto University, 2018); however, we assumed $d = 5$ cm as a representative diameter of the debris flow, which is located in the upper range of reported values. To avoid stopping the debris flow just after initiation, the initial density C_{ini} was set as 0.5 (slightly smaller than C_*). δ_d and δ_e values were set as 0.05 and 0.0007, respectively, according to previous research (Wada et al., 2008). The depth of each initial landslide depth h_{ini} is not dominant for the debris flow scale at the outlet because each debris flow mass develops by eroding 1 m of surface erodible soils and water in the pores. Therefore, h_{ini} was set as 1 m. The initial debris-flow mass was set in the nearest four (2×2) cells of the debris-flow initiation point. The simulation duration is set as 3600 s. The time step Δt was set adaptively using the CFL condition $\Delta t < C_{max} \Delta x / \max(\sqrt{u^2 + v^2} + \sqrt{2gh})$, where C_{max} is the maximum Courant number. Because this numerical method employs the explicit method, $C_{max} = 0.1$ was adopted to avoid numerical instability.

Several assumptions are made in this simulation: all debris flows initiate simultaneously; all soils are initially completely saturated; erodible soil depth is limited to 1 m in all regions; debris flow material has homogeneous grains; and only water, and not additional rainfall, in the soil layer is considered.

3.2 | Calculation results

The maximum water level wl_{max} and topographic change Δz_b (i.e., erosion/deposition) are critical variables for representing the effect caused by the inundation of sediment-laden flood. These factors were determined by the relative water level and ground surface elevations from the initial ground surface, respectively. Figure 4(a, b) shows the maximum water level during the simulation and final topographic change, respectively. A rough comparison reveals that the distribution of each variable agrees with the disaster trace shown in Figure 3(a).

For quantitative comparisons, we selected domain 1, shown in Figure 3(c), as the whole domain, except for the area which has an external catchment, to neglect any areas outside the target area that might be affected by the phenomenon. Note that the cloud area that lacks ground truth is also neglected here. Domain 2, the Akatani river catchment, the main internal catchment in the target domain, was also selected as the target. The available trace data (shown in Figure 3(a)) were categorised into flooded and landslide areas. The trace was obtained by

manual categorisation by interpreting an aerial photograph provided by the Geospatial Information Authority of Japan (2017), suggesting that the data included areas with decreases and increases in elevation (erosion and deposition, respectively) and water-covered (inundated) areas. It is unknown how "landslide" and "flood" area were separated on these aerial photographs. However, according to the data, classification may have relied on the original land use, that is, traces on mountain slope are termed "landslide" and traces on plane areas are termed "flood." To account for this, three binary maps (flooded, landslide, and both) were compared to obtain the "true" map. To obtain a predictive map, three thresholds using the maximum water level and terrain surface deformation were used to produce flooded, landslide, and damaged areas. For each comparison, we calculated the areas for TP (true positive; predicted and occurred), TN (true negative; not predicted and not occurred), FP (false positive; predicted and not occurred), and FN (false negative; not predicted and occurred). Using these values, recall, precision, and threat scores were calculated as TP/(TP + FN), TP/(TP + FP), and (TP + TN)/(TP + FP + FN), respectively. The summary results are shown in Table 1.

The landslide area was first compared to the area in which the simulated absolute terrain deformation value was greater than a threshold value of 0.01 m, as shown in Figure 4(c). The comparison produced a recall value greater than 0.7, both in domains 1 and 2, indicating that the simulated and actual landslide areas mostly coincided.

The flooded area was then compared with the area in which the simulated maximum water level was greater than the threshold value (0.01 m), as shown in Figure 4(d). This result also produced a high recall value (0.741) in domain 2, indicating that the simulated high water level and inundated areas in the internal basin mostly coincided. On the contrary, in domain 1, the recorded recall value (0.570) was much smaller than that domain 2. We note that precision and threat scores cannot be discussed only for landslide or flooded area because there are many FP areas because flooded and landslide areas cannot be separately identified in the simulation.

Finally, the damaged area was determined by comparing the combined flood and landslide area with the area in which the absolute value of Δz_b was greater than 0 m, as this should correspond to locations in which water was present at least once (Figure 4(e)). The recall value was 0.719 in domain 1 and 0.809 in domain 2, where 70–80% of the affected area were actually predicted in the simulation. The precision value was larger than 0.5 in both domains 1 and 2; therefore, the proportion of the actually affected area in the predicted area was smaller than 50%. The threat score, the ratio of TP among TP, FP, and FN, was 0.422 in domain 1 and
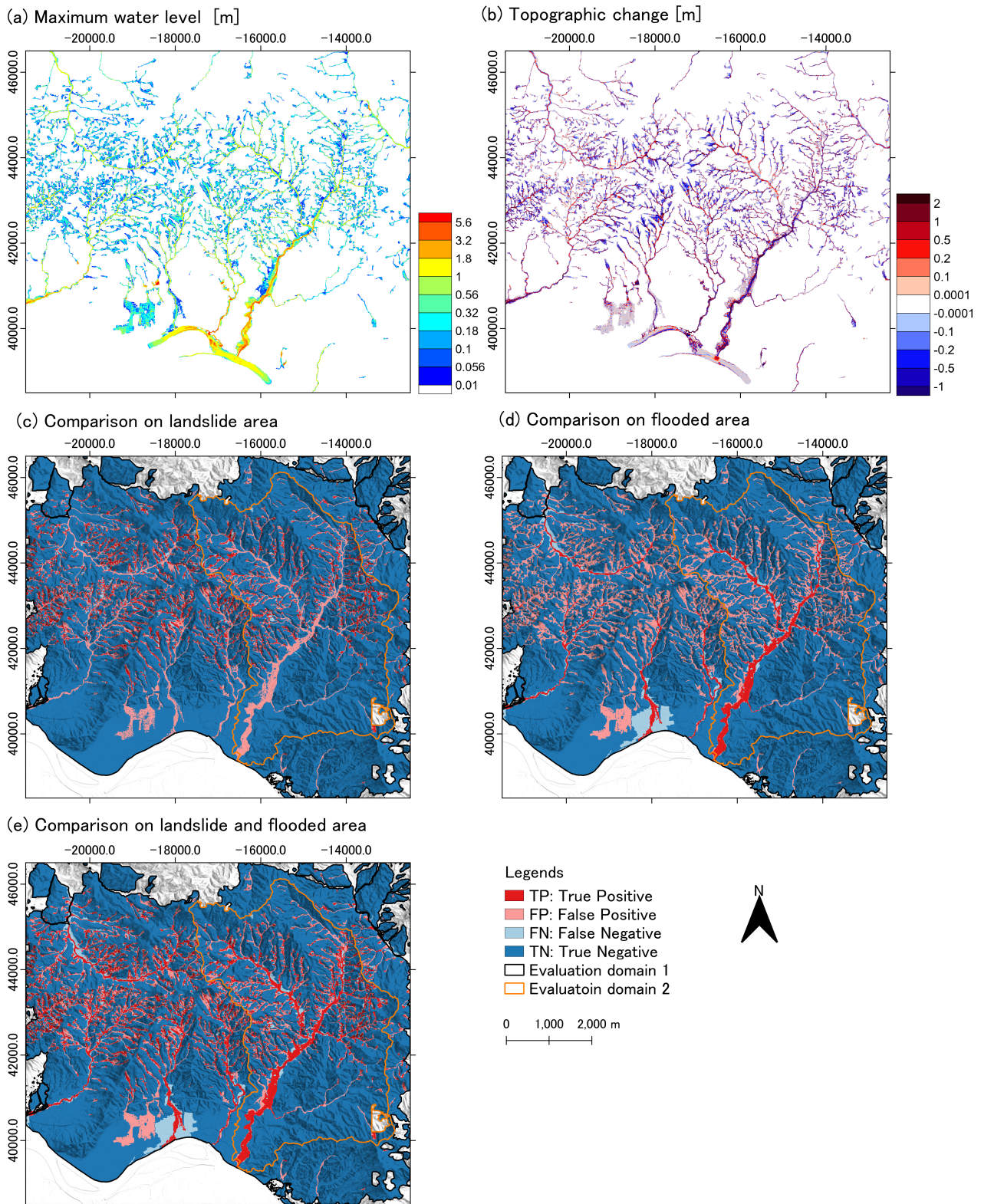
京都大学
KYOTO UNIVERSITY
YAMANOI ET AL.

CIWEM Chartered Institution of Water and Environmental Management

Journal of Flood Risk Management—WILEY

京都大学学術情報リポジトリ
KURENAI 紅
Kyoto University Research Information Repository

9 of 18

FIGURE 4 Calculated reproductive simulation results for (a) maximum water level and (b) topographic change. (c–e) Binary classification results for the quantitative evaluation of simulated results for landslide, flooded, and both (water-covered) areas, respectively. Accuracy, recall, and precision are calculated as (TP + TN)/(TP + TN + FP + FN), TP/(TP + FN), and TP/(TP + FP), respectively. Evaluation domain 1 indicates the area which excludes areas lacking ground truth data and the area that has an external catchment. Evaluation domain 2 indicates the largest internal basin in domain 1

京都大学
KYOTO UNIVERSITY
10 of 18

WILEY—CIWEM
Chartered Institution of
Water and Environmental
Management

Journal of
Flood Risk Management

A Self-archived copy in
Kyoto University Research Information Repository
https://repository.kulib.kyoto-u.ac.jp

京都大学学術情報リポジトリ
KURENAI 紅
Kyoto University Research Information Repository

YAMANOI ET AL.

TABLE 1 Summary of results on simulation reproducibility

Comparison type	Evaluation domain	Recall	Precision	Threat score
Landslide area	Domain 1	0.723	0.365	0.320
Landslide area	Domain 2	0.785	0.252	0.235
Flooded area	Domain 1	0.570	0.166	0.148
Flooded area	Domain 2	0.741	0.325	0.292
Landslide and flooded area	Domain 1	0.719	0.506	0.422
Landslide and flooded area	Domain 2	0.809	0.555	0.490

0.490 in domain 2. According to Figure 4(e), FP and FN areas were categorised into three regions. First, the FP areas appeared along the debris flow traces at the mountain slopes. This is because the debris flow was calculated to be broader than the actual flow. In addition, some debris flows that stopped without further development could not be well reproduced. Second, the FN region appeared along the valleys in the middle stream areas. This result seems to be due a smaller simulated water volume for inundation than that of the actual flow because the simulation considers only water in the soil, but no additional rainfall before or after the debris flow. Finally, both FN and TP areas appeared in the lowland area at the outlet of the valleys. This is also affected by additional rainfall and debris flow stoppings. Additionally, a report pointed out that driftwood and its aggregation (i.e., driftwood jams) at bridges strongly affected the inundation process (Kyoto University, 2018). If we added such processes into the simulation model, the threat score might increase. Notably, the accuracy of the observation area cannot be precisely measured because it was interpreted with the naked eye based on the colours of disaster traces in aerial photograph.

As aforedescribed, the affected area in the simulation showed differences to the actually affected area. However, from the viewpoint of application in disaster prediction work, the recall value is empirically regarded to be important. Because the simulation shows a high recall value, especially in the internal basin (domain 2), we believe that our results are sound, and we leave the improvement of reproducibility for future work.

4 | PREDICTIVE SIMULATION EMPLOYING STATISTICAL LANDSLIDE PREDICTION

4.1 | Statistical landslide prediction model for generating artificial landslide dataset

Debris flow initiation points, that is, slope failures or landslides, are essential inputs in the proposed simulation.

Note that a fully predictive simulation requires data sourced solely from pre-disaster information. However, we assume that the statistical model described below can be obtained in the pre-disaster period.

This study adopts a statistical approach. In selecting the method in the statistical models, probabilistic (i.e., nondeterministic) response variables are preferred for treating variations in the predicted results. Therefore, we used a logistic regression model to derive the initiation point likelihood at each top point in the debris-flow trace. To obtain high-quality predictions, many variables are generally selected as explanatory variables, including curvature, slope, aspect, flow accumulation, elevation, lithology, and precipitation. However, for selecting input variables, data availability is also important to establish the model used for prediction. Additionally, the relationship between landslide occurrence and aspect or elevation is highly location dependent. Therefore, we used only four variables: slope, flow accumulation, and profile/tangential curvature, as shown in Figure 5(a–d). Here, we used 10-m resolution data for landslide prediction to achieve the same quality of the used DEMs.

In this regression, cell by cell with 10-m resolution, we extracted the set of slope θ, flow accumulation area A_a, profile curvature X_p, tangential curvature X_t, and binary value (1 or 0) that expresses whether debris-flow initiation points exist in the corresponding cell. To reduce noise in the elevation data, θ, A_a, X_p, and X_t were used by taking the averages of 5×5 cells (i.e., 50×50 m). The entire target area contained 514,566 data points. Areas with a drainage area outside the target area, or whose land use is not forest, were neglected because landslides generally rarely occur in such areas. The 10-m resolution land use and land cover map (Japan Aerospace Exploration Agency, 2016) are used for this classification. In the logistic regression, possibility p that debris flow initiates at the corresponding cell is calculated as

$$p = \frac{e^{\alpha_0 + \alpha_1\theta + \alpha_2 A_a + \alpha_3 X_p + \alpha_4 X_t}}{1 + e^{\alpha_0 + \alpha_1\theta + \alpha_2 A_a + \alpha_3 X_p + \alpha_4 X_t}} \tag{13}$$

From the regression for the entire domain of the target area, $\alpha_0 - \alpha_4$ were obtained as shown in Table 2. In Wald's
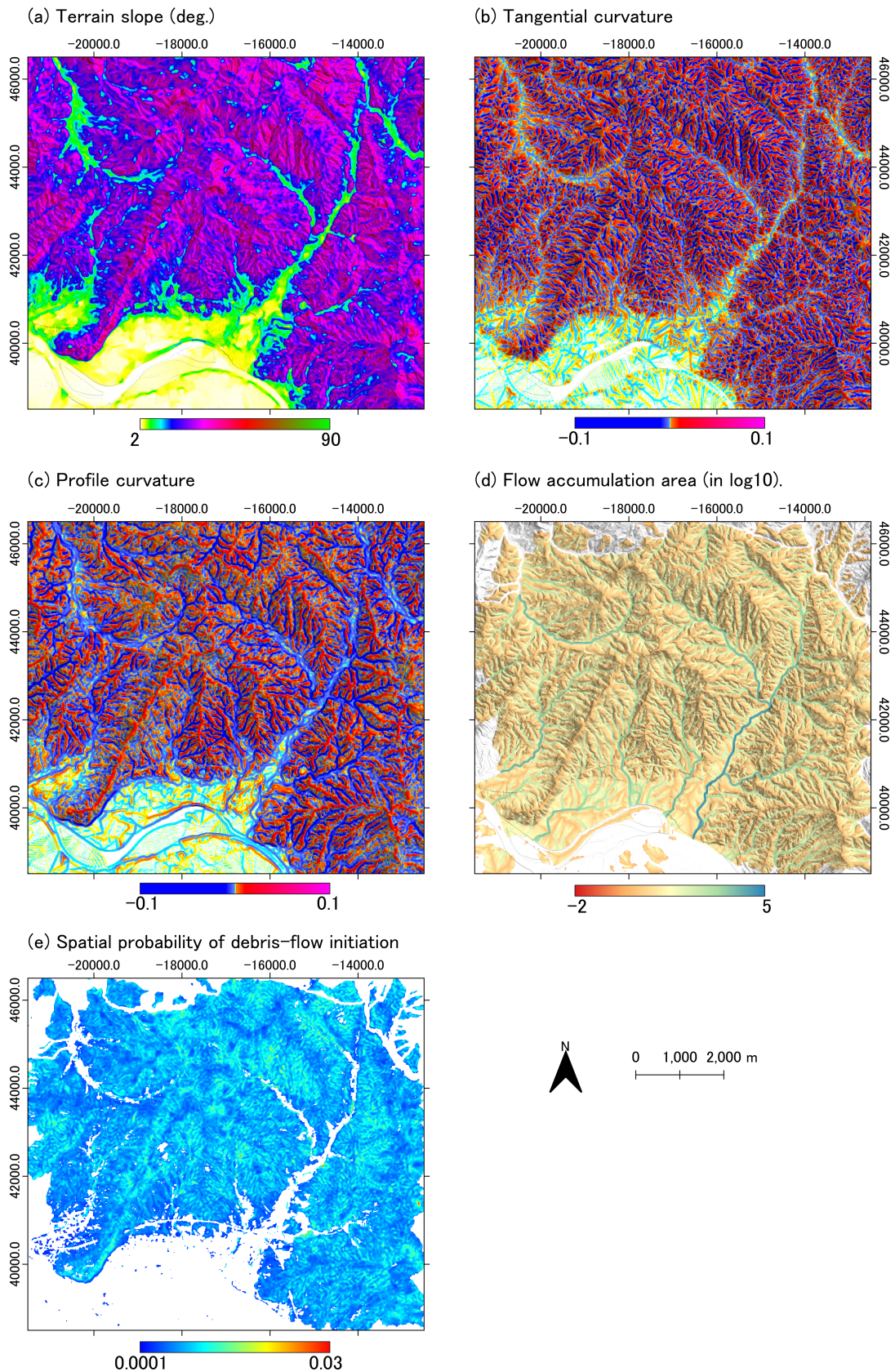
京都大学
KYOTO UNIVERSITY
YAMANOI ET AL.

A Self-archived copy in
Kyoto University Research Information Repository
https://repository.kulib.kyoto-u.ac.jp

CIWEM Chartered Institution of   Journal of
Water and Environmental   Flood Risk Management—WILEY
Management

京都大学学術情報リポジトリ
KURENAI 紅
Kyoto University Research Information Repository
11 of 18

FIGURE 5 Input (a–d) and output (e) variables of logistic regression: (a) terrain slope (°), (b) tangential and (c) profile curvature, (d) common logarithm of flow accumulation area (m^2), and (e) by-point regression-obtained spatial probability of debris-flow initiation. (a–d) are calculated using 10-m-resolution DEM. Each value is the average of all neighbours within a five-cell range

京都大学
KYOTO UNIVERSITY

	Estimated value	Standard error	z value	*p* value for (>|z|) in Wald's test
α_0	−6.517527	0.090660	−71.890	<2e-16
α_1	0.043171	0.002619	16.484	<2e-16
α_2	0.416436	0.035190	11.834	<2e-16
α_3	24.769787	3.565543	6.947	3.73e-12
α_4	21.979709	2.617267	8.398	<2e-16

TABLE 2 Logistic regression results ($n = 514{,}566$)
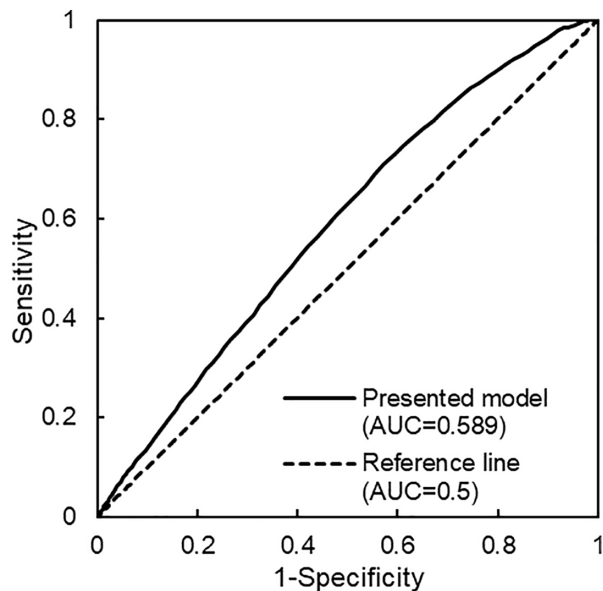
FIGURE 6 Receiver operating characteristic (ROC) curve for the presented logistic model for landslide prediction

test, the p value was small, implying that θ, A_a, X_p, and X_t are dominant for p. Figure 5(e) shows the predicted probabilities at the 10-m resolution. They ranged from 0.001 to 0.035, which does not predict a specific location; nonetheless, we use this result for debris-flow prediction considering the hypothesis that the required landslide-prediction accuracy is not high. The estimated p was relatively low in the bottom of channel streams and relatively high in the lower portion of slopes besides the streams. This is due to the larger value of slopes θ and profile curvatures X_p at the portion. The estimated coefficient for tangential curvature α_3 was positive, thus agreeing with the fact that landslides likely occurred in ridge-like terrains (Danjo et al., 2018).

The receiver operating characteristic curve for this model can be obtained as shown in Figure 6, by plotting the sensitivity (TP/[TP + FN]) and 1-specificity (1-TN/[TN + FP]) as the change in the cut-off probability. Here, TP, TN, FP, and FN were obtained cell-by-cell. The area under curve (AUC) value was 0.589; therefore, the performance of this model in predicting the specific location was lower than that reported in previous studies

(e.g., 0.80–0.84; Gorsevski et al., 2006; 0.78 ± 0.03; Ozturk et al., 2021). This is not surprising because this simple model employs relatively small training domains, neglects climate- and geography-related variables, and employs a relatively high resolution (i.e., 10 m). According to the AUC the presented model is better than the random classifier (AUC = 0.5). We used this model to show that high-performance models for landslide prediction are not always required for application in debris-flow prediction.

To enable simulation inputs, the spatial probability map had to be converted into landslide maps. Hence, we generated pseudorandom real numbers between zero and one for all cells in target areas. For results smaller than the corresponding cell probabilities, the cell was selected as a debris-flow initiation point. For example, if a 10 m × 10 m cell had a probability value of 0.005 and the generated pseudorandom number was 0.003 (<0.005), it was selected as a debris-flow initiation point. By changing the random-seed generator, 60 sets of debris-flow initiation points were created; these are partially shown in Figure 7(a,b). Consequently, the mean number of generated points was 3518.3, and the standard deviation (SD) was 63.7 in the entire domain. The actual landslide number was 3721, which is slightly larger than the statistically estimated value. However, the actual number includes landslides that occurred in nonforest areas or areas with external catchments, which cannot be predicted using this method. The number in the predictable area was 3598, which is approximately in the range of the proposed estimation.

The abovementioned method can provide the probability distribution of debris-flow initiation points in a target area for a target event. This model can be considered a probability model for a disaster of similar magnitude in a similar region. Therefore, it cannot directly be applied to different magnitudes or regions with different lithology and/or climate characteristics. We do not discuss the applicability of the proposed regression model. However, similar disasters in other regions can yield a similar probability function through logistic regression. Therefore, by archiving the debris-flow initiation point and topography, lithology, and precipitation data, the quality of the regression model can be improved in the future. In Japan,
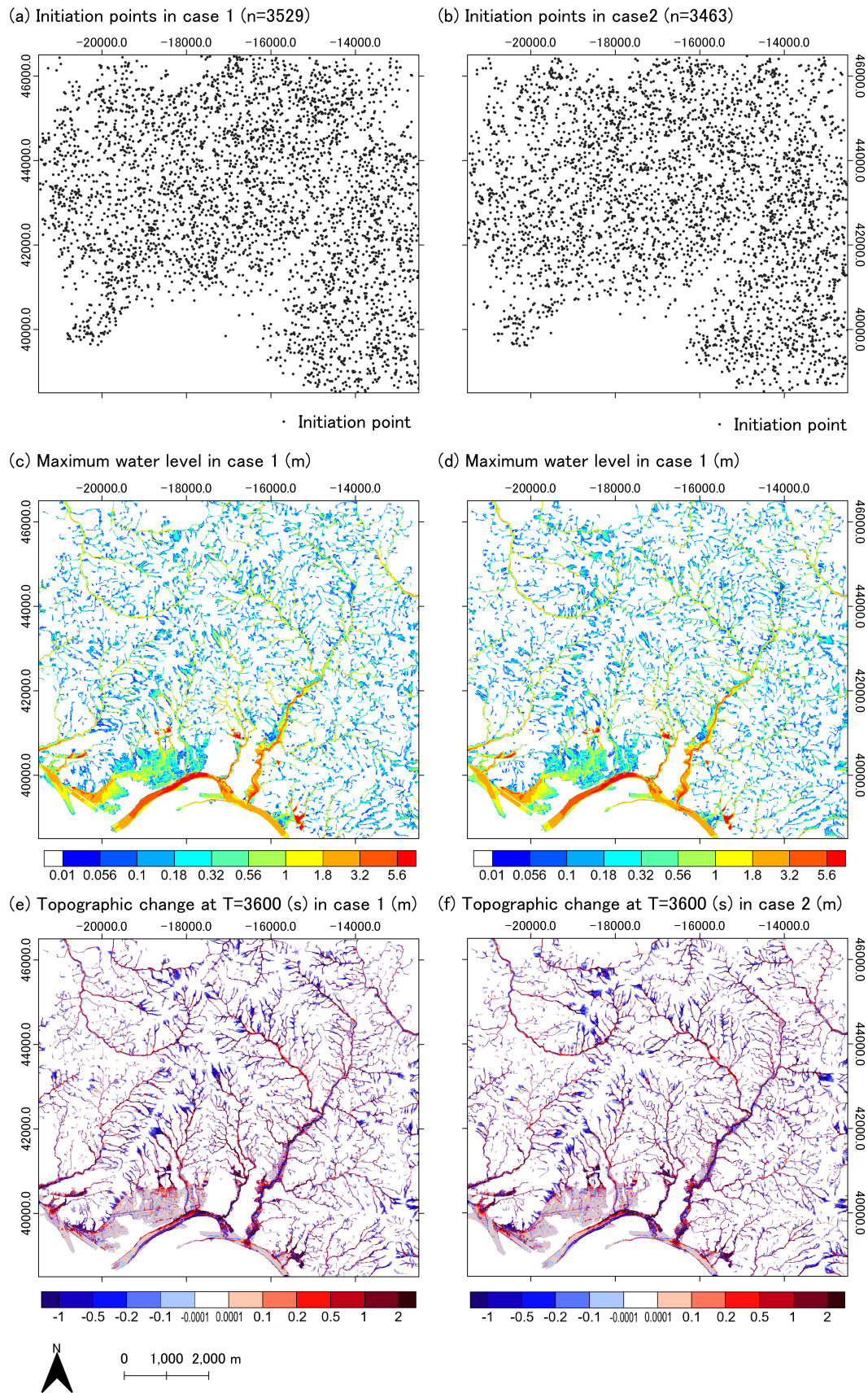
京都大学
KYOTO UNIVERSITY
YAMANOI ET AL.

A Self-archived copy in
Kyoto University Research Information Repository
https://repository.kulib.kyoto-u.ac.jp

CIWEM Chartered Institution of   Journal of
        Water and Environmental   Flood Risk Management—WILEY
        Management

京都大学学術情報リポジトリ
KURENAI 紅
Kyoto University Research Information Repository
13 of 18

FIGURE 7   (a,b) Generated debris-flow initiation point datasets; (c,d) calculated maximum water level results ($T = 3600$ s); and (e,f) calculated topographic change results ($T = 3600$ s). Only Cases 1–2 are shown

similar sediment-related disasters occur almost every year; therefore, this method could be applied widely for prediction if we have sufficient data. We do not introduce a precipitation-related index because slope failures are evenly distributed in the target event. However, such an index could be introduced theoretically. Additionally, the required accuracy of the probability function is not always high as described below.

4.2 | Multicase predictive simulation using artificial landslide datasets

Sixty simulation cases (in light of available resources) were analysed using the artificial debris-flow initiation points as input data. Other than the initiation points, all conditions, parameters, topographic conditions, simulation models, and discretisation methods were the same as those in the reproductive simulation described in Section 3. Figure 7(c–f) shows some obtained maximum water levels and topographic changes. Approximately similar maximum water level and topographic change values are found in the downstream area, suggesting that damage here is not sensitive to the debris-flow initiation point distribution. By contrast, high variability is observed in the upstream area closer to the debris-flow initiation points. The variability among the 60 results was quantified using the averaged value (AVE) and SD; relative SD (RSD; $=SD/|AVE|$)) values were calculated for maximum water level and terrain deformation (Figure 8(a–d)).

Figure 8(a,c,e) shows the AVE, SD, and RSD for the maximum water level, respectively. At the outlets of debris-flow prone valleys, AVE is 0.5–1.0 m; at valley bottoms in downstream areas, AVE is 1.0–3.0 m, indicating a general increase as streams flow downstream. By contrast, SD shows only modest variations between 0.0 and 0.2 m in Figure 8(c). Thus, RSD ($=SD/|AVE|$) is relatively larger upstream and smaller downstream. By contrast, areas around the outlets of small debris-flow-prone streams have RSDs of ∼0.5–1.0, indicating a higher degree of predicted-damage uncertainty. In the flood plain along the mainstream of Chikugo river, RSD values were higher in some portions, especially along the mountain front. This mountain front does not have a watershed-like topography; the debris flow effect, therefore, depends on whether landslides take place on the nearby slope. Accordingly, water flow appeared only in a small number of simulation cases among the 60 cases, resulting in a large RSD value. Note that higher RSD values appeared in the mainstream of Chikugo river. This is because the simulated distance the flood water travelled does not completely match each other in the

60 cases since the simulation stops after 3600 s. In an actual situation, such areas should be filled with river water, which, however, could not be simulated with our approach. Figure 8(b,d,f) shows the SD, AVE, and RSD values for topographic changes, respectively. Each index follows a trend similar to the corresponding maximum water level index, although RSD in the residential area at the valley bottom is slightly larger than that for maximum water level.

5 | DISCUSSION

In the proposed method, debris flow inundation levels and topographic changes were successfully simulated from observed and statistically predicted slope failure data. The results show that hazards, their affected areas, and the uncertainty are predicted precisely from the statistical model. If such a statistical model is available before the disaster, the affected area can be considered predictable. Additionally, our results indicated that the uncertainty (i.e., RSD) decreases as debris flows downstream in the watershed-like topography. Therefore, inundation and topographic changes in the valley bottom and downstream alluvial area can be simulated if the landslide location changes. By contrast, large RSD values appeared in upstream and flood plain areas near steep slopes. This result implies that hazard predictability highly depends on the topography, where valley bottoms and downstream alluvial areas have relatively high predictability. This result also implies that the debris flow effect in such areas might be predicted even if the landslide prediction accuracy is not remarkably high. This conclusion is also supported by the fact that a simple landslide prediction model with a relatively low performance was used for this simulation.

However, this study has several limitations. First, numerical experiments were conducted for dense landslides (>3000 debris-flow initiation points over 72 km^2). Tests under lower-density conditions might increase the uncertainty, even in downstream areas, because not all debris flows might accumulate. Further, as noted in the Section 3, this simulation relies on several assumptions. For example, all debris flows are considered to initiate simultaneously in this simulation. If the initiation time varies, the accumulation effect might change and increase the uncertainty. Further studies are required to clarify how such assumptions influence the uncertainty and predictability of hazards. Despite these limitations, if there is sufficient water to develop a debris flow, sufficient density of slope failure for multiple debris flows to join, and the range of debris-flow initiation timings is small, precise simulations are possible. From a practical
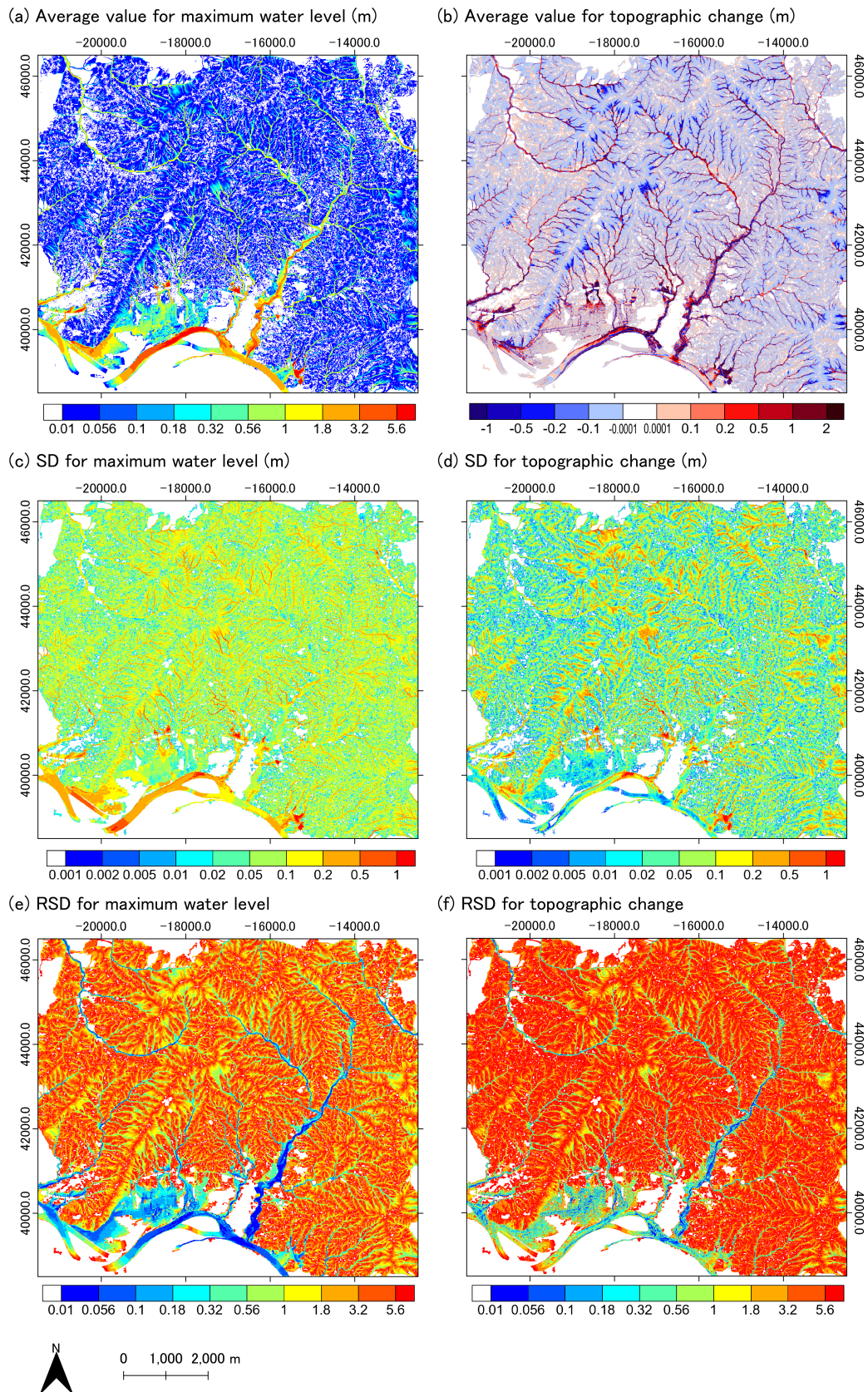
FIGURE 8 (a,c,e) Average value, standard deviation (SD), and relative standard deviation (RSD) for maximum water level, respectively. (b,d,f) Average value, SD, and RSD for topographic change, respectively

16 of 18 | **WILEY—CIWEM** Chartered Institution of Water and Environmental Management *Journal of* Flood Risk Management

京都大学 KYOTO UNIVERSITY

A Self-archived copy in
Kyoto University Research Information Repository
https://repository.kulib.kyoto-u.ac.jp

京都大学学術情報リポジトリ
KURENAI 紅
Kyoto University Research Information Repository

YAMANOI ET AL.

perspective, if an appropriate statistical model for the target scale is used, we can precisely and quantitatively estimate the affected area, affected degrees, and uncertainty. We believe that this represents significant progress in disaster assessment studies.

It is important to note that this paper mainly discusses influences of the initiation point location to the predicted affected area, not the simulation quality itself. We neglect aspects such as additional rainfall, the effect of driftwood, and buildings. Additionally, fundamental soil properties, such as grain size, may also affect the prediction. Simulations including such parameters should improve predictability in some regions.

6 | CONCLUSIONS

This study proposed a 2D debris-flow simulation scheme from initiation points and discussed the slope failure condition settings needed to predict debris flows and sediment-laden flooding. As accurate slope failure prediction is difficult using current techniques, we proposed a predictive simulation method that does not require accurate landslide prediction (i.e., conventional statistics-based landslide prediction). We generated artificial debris-flow initiation points using the spatial probability of slope failure and pseudorandom numbers to change the slope failure location based on the random seed. In convergent catchment topographies, individual debris flows merge as they flow downstream. Under such conditions, different debris-flow initiation points result in similar affected locations. To quantify the similarities, we calculated the RSD of 60 cases with different random seeds. The RSD decreased in downstream regions with large drainage areas.

Our results suggest the following. The damage produced by debris flows or sediment-laden floods in the downstream regions of watershed-like topographies is predictable under the presented conditions regardless of the location of sediment sources (slope failures). The dominant factors in terms of predictability are the presence of a catchment-like concave topography, sufficient water to develop a debris flow, and sufficient density of slope failure for multiple debris flows to join. Thus, for concave topographies, it is possible to predictively simulate the inundation when high rainfall yields multiple slope failures and debris flows.

Further studies will be required to estimate how each assumption in the simulation affects these conclusions. However, this study demonstrated the effectiveness of using high-performance computing for multicase simulation to evaluate the effects of debris-flow initiation locations. A similar approach involving changing each

condition will be used in a future study to quantitatively evaluate each assumption.

DATA AVAILABILITY STATEMENT

Data supporting the study findings are available from Geospatial Information Authority of Japan. Restrictions apply to the availability of these data, which were used under license for this study. Data are available at https://www.gsi.go.jp/kiban/ and https://www.gsi.go.jp/BOUSAI/H29hukuoka_ooita-heavyrain.html with the permission of Geospatial Information Authority of Japan. The simulation code presented in this paper is available from the archive http://doi.org/10.5281/zenodo.4655227.

ORCID
Kazuki Yamanoi https://orcid.org/0000-0002-2837-2522

REFERENCES

An, H., Viet, T. T., Lee, G., Kim, Y., Kim, M., Noh, S., & Noh, J. (2016). Development of time-variant landslide-prediction software considering three-dimensional subsurface unsaturated flow. *Environmental Modelling and Software*, *85*, 172–183. https://doi.org/10.1016/j.envsoft.2016.08.009

Bao, Y., Chen, J., Sun, X., Han, X., Li, Y., Zhang, Y., Gu, F., & Wang, J. (2019). Debris flow prediction and prevention in reservoir area based on finite volume type shallow-water model: A case study of pumped-storage hydroelectric power station site in Yi County, Hebei, China. *Environmental Earth Sciences*, *78*(19), 577. https://doi.org/10.1007/s12665-019-8586-4

Chen, H. X., Zhang, L. M., Gao, L., Yuan, Q., Lu, T., Xiang, B., & Zhuang, W. L. (2017). Simulation of interactions among multiple debris flows. *Landslides*, *14*(2), 595–615.

Chikugo River Office. (n.d.). Inundation hazardous areas. Retrieved from http://www.qsr.mlit.go.jp/chikugo/bousai/shinsuisoutei/index.html

Christen, M., Kowalski, J., & Bartelt, P. (2010). RAMMS: Numerical simulation of dense snow avalanches in three-dimensional terrain. *Cold Regions Science and Technology*, *63*(1–2), 1–14. https://doi.org/10.1016/j.coldregions.2010.04.005

京都大学
KYOTO UNIVERSITY
YAMANOI ET AL.

A Self-archived copy in
Kyoto University Research Information Repository
https://repository.kulib.kyoto-u.ac.jp

CIWEM
Chartered Institution of
Water and Environmental
Management

Journal of
Flood Risk Management—WILEY

京都大学学術情報リポジトリ
KURENAI 紅
Kyoto University Research Information Repository

17 of 18

D'Agostino, V., & Tecca, P. (2006). Some considerations on the application of the FLO-2D model for debris flow hazard assessment. *WIT Transactions on Ecology and the Environment*, *90*, 159–170. https://doi.org/10.2495/DEB060161

Danjo, T., Ishizawa, T., & Kimura, T. (2018). Spatial analysis of the landslide characteristics caused by heavy rainfall in the northern Kyushu district in July, 2017 using topography, geology, and rainfall levels. *Journal of Disaster Research*, *13*(5), 832–845. https://doi.org/10.20965/jdr.2018.p0832

Frank, F., McArdell, B. W., Huggel, C., & Vieli, A. (2015). The importance of entrainment and bulking on debris flow runout modeling: Examples from the Swiss Alps. *Natural Hazards and Earth System Sciences*, *15*(11), 2569–2583. https://doi.org/10.5194/nhess-15-2569-2015

Fukuoka Prefecture. (2018). Report on the verification of disaster response to the July 2017 heavy rainfall in Northern Kyushu. Retrieved from https://www.bousai.pref.fukuoka.jp/spc/images/H29hokubugouu.pdf

Fukuoka Prefecture. (n.d.). Map for sediment-related disaster warning area. Retrieved from http://www2.sabomap.jp//fukuoka/

Gao, L., Zhang, L. M., Chen, H. X., & Shen, P. (2016). Simulating debris flow mobility in urban settings. *Engineering Geology*, *214*, 67–78. https://doi.org/10.1016/j.enggeo.2016.10.001

George, D. L., & Iverson, R. M. (2014). A depth-averaged debris-flow model that includes the effects of evolving dilatancy. II. Numerical predictions and experimental tests. *Proceedings of the Royal Society A, Mathematical, Physical and Engineering Sciences*, *470*(2170), 20130820. https://doi.org/10.1098/rspa.2013.0820

Geospatial Information Authority of Japan. (2017). Information related to the Northern Kyushu heavy rainfall disaster in July 2017. Retrieved from https://www.gsi.go.jp/BOUSAI/H29hukuoka_ooita-heavyrain.html

Geospatial Information Authority of Japan (n.d.). Digital map (basic geospatial information). Retrieved from https://www.gsi.go.jp/kiban/

Gorsevski, P. V., Gessler, P. E., Foltz, R. B., & Elliot, W. J. (2006). Spatial prediction of landslide hazard using logistic regression and ROC analysis. *Transactions in GIS*, *10*, 395–415. https://doi.org/10.1111/j.1467-9671.2006.01004.x

Han, X., Chen, J., Xu, P., Niu, C., & Zhan, J. (2018). Runout analysis of a potential debris flow in the Dongwopu gully based on a well-balanced numerical model over complex topography. *Bulletin of Engineering Geology and the Environment*, *77*(2), 679–689. https://doi.org/10.1007/s10064-017-1079-3

Hinokidani, O. (1998a). Numerical method for two-dimensional bed-level variation (part-1). *Journal of the Japan Society of Erosion Control Engineering*, *50*(5), 82–88. https://doi.org/10.11475/sabo1973.50.5_82

Hinokidani, O. (1998b). Numerical method for two-dimensional bed-level variation (part-2). *Journal of the Japan Society of Erosion Control Engineering*, *50*(6), 70–76. https://doi.org/10.11475/sabo1973.50.6_70

Hungr, O., Leroueil, S., & Picarelli, L. (2014). The Varnes classification of landslide types, an update. *Landslides*, *11*, 167–194. https://doi.org/10.1007/s10346-013-0436-y

Hungr, O., & McDougall, S. (2009). Two numerical models for landslide dynamic analysis. *Computers and Geosciences*, *35*(5), 978–992. https://doi.org/10.1016/j.cageo.2007.12.003

Hussin, H. Y., Quan Luna, B., van Westen, C. J., Christen, M., Malet, J.-P., & van Asch, T. W. J. (2012). Parameterization of a numerical 2-D debris flow model with entrainment: A case study of the Faucon catchment, Southern French Alps. *Natural Hazards and Earth System Sciences*, *12*, 3075–3090. https://doi.org/10.5194/nhess-12-3075-2012

Iverson, R. M., & George, D. L. (2014). A depth-averaged debris-flow model that includes the effects of evolving dilatancy. I. Physical basis. *Proceedings of the Royal Society A, Mathematical, Physical and Engineering Sciences*, *470*, 20130819. https://doi.org/10.1098/rspa.2013.0819

Japan Aerospace Exploration Agency. (2016). High-resolution land use and land cover map of Japan (released in September 2016/version 16.09). Retrieved from https://www.eorc.jaxa.jp/ALOS/en/lulc/lulc_jpn.htm

Kyoto University. (2018). Report on the July 2017 heavy rainfall in Northern Kyushu. Retrieved from http://www.dpri.kyoto-u.ac.jp/web_j/publication/other/20180330_kyusyu.pdf

Melo, R., Van Asch, T., & Zêzere, J. L. (2018). Debris flow run-out simulation and analysis using a dynamic model. *Natural Hazards and Earth System Sciences*, *18*(2), 555–570. https://doi.org/10.5194/nhess-18-555-2018

Naef, D., Rickenmann, D., Rutschmann, P., & McArdell, W. B. (2006). Comparison of flow resistance relations for debris flows using a one-dimensional finite element simulation model. *Natural Hazards and Earth System Sciences*, *6*(1), 155–165. https://doi.org/10.5194/nhess-6-155-2006

Nakatani, K., Hayami, S., Satofuka, Y., & Mizuyama, T. (2016). Case study of debris flow disaster scenario caused by torrential rain on Kiyomizudera, Kyoto, Japan—Using hyper KANAKO system. *Journal of Mountain Science*, *13*(2), 193–202. https://doi.org/10.1007/s11629-015-3517-7

O'Brien, J. S., & Julien, P. Y. (1985). Physical processes of hyper-concentrated sediment flows. In: Proceedings of the ASCE Specialty Conference on the Delineation of Landslides, Floods, and Debris Flow Hazards in Utah. Utah Water Research Laboratory. Series UWRL/g-85/03, pp. 260–279.

O'Brien, J. S., Julien, P. Y., & Fullerton, W. T. (1993). Two-dimensional water flood and mudflow simulation. *Journal of Hydraulic Engineering*, *119*(2), 244–261. https://doi.org/10.1061/(ASCE)0733-9429(1993)119:2(244)

OpenStreetMap Contributors. (2020). Planet dump. Retrieved from https://planet.osm.org

Ozturk, U., Pittore, M., Behling, R., Roessner, S., Andreani, L., & Korup, O. (2021). How robust are landslide susceptibility estimates? *Landslides*, *18*, 681–695. https://doi.org/10.1007/s10346-020-01485-5

Raia, S., Alvioli, M., Rossi, M., Baum, R. L., Godt, J. W., & Guzzetti, F. (2014). Improving predictive power of physically based rainfall-induced shallow landslide models: A probabilistic approach. *Geoscientific Model Development*, *7*(2), 495–514. https://doi.org/10.5194/gmd-7-495-2014

Reichenbach, P., Rossi, M., Malamud, B. D., Mihir, M., & Guzzetti, F. (2018). A review of statistically-based landslide susceptibility models. *Earth-Science Reviews*, *180*, 60–91. https://doi.org/10.1016/j.earscirev.2018.03.001

Revellino, P., Hungr, O., Guadagno, F. M., & Evans, S. G. (2004). Velocity and runout simulation of destructive debris flows and debris avalanches in pyroclastic deposits, Campania region,

Italy. *Environmental Geology*, *45*(3), 295–311. https://doi.org/10.1007/s00254-003-0885-z

Rickenmann, D. (1999). Empirical relationships for debris flows. *Natural Hazards*, *19*(1), 47–77. https://doi.org/10.1023/a:1008064220727

Rickenmann, D., Laigle, D., McArdell, B. W., & Hübl, J. (2006). Comparison of 2D debris-flow simulation models with field events. *Computational Geosciences*, *10*(2), 241–264. https://doi.org/10.1007/s10596-005-9021-3

Rodríguez-Morata, C., Villacorta, S., Stoffel, M., & Ballesteros-Canovas, J. A. (2019). Assessing strategies to mitigate debris-flow risk in Abancay province, south-central Peruvian Andes. *Geomorphology*, *342*, 127–139. https://doi.org/10.1016/j.geomorph.2019.06.012

Salvatici, T., Morelli, S., Pazzi, V., Frodella, W., & Fanti, R. (2017). Debris flow hazard assessment by means of numerical simulations: Implications for the Rotolon creek valley (northern Italy). *Journal of Mountain Science*, *14*, 636–648. https://doi.org/10.1007/s11629-016-4197-7

Schraml, K., Thomschitz, B., Mcardell, B. W., Graf, C., & Kaitna, R. (2015). Modeling debris-flow runout patterns on two alpine fans with different dynamic simulation models. *Natural Hazards and Earth System Sciences*, *15*(7), 1483–1492. https://doi.org/10.5194/nhess-15-1483-2015

Takahashi, T. (2007). *Debris flow: Mechanics, prediction and countermeasures*. Taylor & Francis.

Takahashi, T., & Nakagawa, H. (1991). Prediction of stony debris flow induced by severe rainfall. *Journal of the Japan Society of Erosion Control Engineering*, *44*, 12–19. https://doi.org/10.11475/sabo1973.44.3_12

van Asch, T. W., Tang, C., Alkema, D., Zhu, J., & Zhou, W. (2014). An integrated model to assess critical rainfall thresholds for run-out distances of debris flows. *Natural Hazards*, *70*(1), 299–311. https://doi.org/10.1007/s11069-013-0810-z

Wada, T., Satofuka, Y., & Mizuyama, T. (2008). Integration of 1- and 2-dimensional models for debris flow simulation. *Journal of the Japan Society of Erosion Control Engineering*, *61*(2), 36–40. https://doi.org/10.11475/sabo.61.2_36

Wu, J., Chen, G., Zheng, L., & Zhang, Y. (2013). GIS-based numerical modelling of debris flow motion across three-dimensional terrain. *Journal of Mountain Science*, *10*(4), 522–531. https://doi.org/10.1007/s11629-013-2486-y